Understanding the reaction mechanisms involving weakly bound ^{6}Li with ^{209}Bi

S. Santra*
Nuclear Physics Division, Bhabha Atomic Research Centre, Mumbai - 400085, INDIA

Extensive measurements on the cross sections for elastic, inelastic, transfer and inclusive as well as exclusive breakup channels in ^{6}Li+^{209}Bi reaction were made at energies near the Coulomb barrier in the range of $E_{lab} = 24 - 50$ MeV. A simultaneous description of all these channels (that put severe constraints on the potential and coupling parameters) has been made through the coupled-channels calculations. Optical model (OM) analysis of the elastic scattering data shows the absence of the normal threshold anomaly in the real potential, and the existence of non-zero imaginary potential even at deep sub-barrier energies. Effective (bare+polarization) potentials generated due to the coupling of breakup channels were found to reproduce the observed energy dependence of the OM potentials. Exclusive measurements show that the sequential breakup of ^{6}Li ($\rightarrow \alpha + d$) through its unbound resonant (3^{+}, 2.18 MeV) state is most dominant followed by ^{6}Li$\rightarrow^{5}$Li$\rightarrow \alpha + p$ breakup. Inclusive alpha cross section was found to be the major reaction channel particularly at sub-barrier energies where it exhausts almost all of the total reaction cross section. An investigation for the origin of such a large inclusive alpha production cross section reveals that most of the alpha particles are due to breakup, where either the complementary breakup fragment i.e. d is captured and α is emitted or both of the fragments are emitted.

1. Introduction

Study of reactions involving weakly bound projectiles at energies around the Coulomb barrier has been very interesting because of the observation of many new features compared to the ones involving tightly bound projectiles. Understanding the reaction mechanisms of loosely bound projectiles with target nuclei and the effect of breakup coupling on various outgoing channels is very important, because of its application to the determination of radiative capture cross section [1] of astrophysical interest and the quest for super heavy elements by the fusion of nuclei near the drip line.

The effect of coupling between the relative motion and the intrinsic degrees of freedom of the participating nuclei is manifested as "Threshold Anomaly" in the energy dependence behavior of the real part of the effective interaction potential [2]. Although this behavior is observed for most of the reactions involving strongly bound stable projectiles, for example, ^{12}C+^{208}Pb,^{209}Bi[3, 4], it may not be true for the reactions involving loosely-bound projectiles with large breakup probability, for example, ^{6}Li+^{208}Pb[5], ^{6}Li+^{138}Ba[6], ^{6}Li+^{59}Co[7], ^{6}Li+^{28}Si[8], ^{9}Be+^{209}Bi[9], ^{9}Be+^{64}Zn[10, 11]. For the latter systems, there is no pronounced energy dependence of the real potential, and at energies below the Coulomb barrier the imaginary potential is found to remain constant or sometimes increases with the lowering of energy. The increase in the imaginary potential below the Coulomb barrier is sometimes associated with a slight decrease in the real potential. Hussein *et al.* have showed that this behavior is a new manifestation of the dispersion relation and named it as the "Breakup threshold anomaly"[12]. Though threshold anomaly still exists for ^{7}Li [5–8], it is not observed in many reactions involving ^{6}Li and ^{9}Be [5–11]. However, contradictory results exist involving same weakly bound projectiles, e.g., Signorini *et al.* did not observe any threshold anomaly for ^{9}Be+^{209}Bi [9], while Woolliscroft *et al.* saw a pronounced

*Electronic address: ssantra@barc.gov.in

threshold anomaly for a very similar system ^{9}Be+^{208}Pb [13]. It implies that a clear understanding of the effect of breakup on the energy dependence of the optical potential is still elusive. Systematic studies of more reactions involving weakly bound projectiles are necessary to unfold these effects.

The observation of a large cross section for inclusive α produced by breakup and different transfer channels for reactions involving weakly bound projectiles with cluster structure '$\alpha + x$' is well established [14–21]. Kelly *et al.*, in a study for ^{6,7}Li+^{208}Pb reaction [14], have shown that the cross sections for exclusive breakup of ^{6}Li(^{7}Li) into α+$d(t)$ are much lower than the measured inclusive α. They suggested that α produced from transfer channels could be very important. Castaneda *et al.*[22] in their detailed work on ^{6}Li+^{197}Au reaction have found that these alpha can be produced by direct as well as sequential processes. They have observed that almost 50% of the inclusive alpha can be explained in terms of ^{6}Li$\rightarrow\ \alpha + d$ and ^{6}Li$\rightarrow^{5}$Li$\rightarrow\ \alpha + p$ exclusive breakup channels. The origin of the remaining cross sections were not clear. In a similar study for ^{6}Li+^{208}Pb system, Signorini *et al.*[17] have found that the combined cross sections of exclusive breakup of ^{6}Li into $\alpha + d$ and $1n$-stripping followed by breakup (^{6}Li$\rightarrow^{5}$Li$\rightarrow\ \alpha + p$) also cannot explain the large cross section for inclusive α. They suggested many other possible channels that might contribute to the rest of the α particles. Partial fusion or stripping breakup is one of the important channels. So, it would be highly interesting to estimate the α contribution from all of the above channels including the partial fusion and explain the measured inclusive α for the present system ^{6}Li+^{209}Bi. Exclusive measurements of alpha particles are essential to delineate different processes leading to such a large inclusive cross section and to understand the effect of projectile breakup on other channels.

Breakup being one of the reaction channels, its coupling with the elastic channel may lead to enhancement of complete fusion (CF), showing up the threshold anomaly. Alternatively, the breakup of the projectile before reaching the fusion barrier will lead to loss of flux and hence the CF should be reduced [23]. Thus the coupling mechanism will be best understood when the same set of potential parameters are used in the coupled-channels calculations to understand both the elastic and the fusion data simultaneously. In addition, if the couplings and potential parameters are unique then the coupled-channels (CC) calculations are expected to reproduce the cross sections for other non-elastic channels too. It is a difficult task firstly because one needs to measure the cross sections for all the above channels and secondly one has to find a unique parameter set that describe them through the same CC calculations. Since both the CF and ICF (incomplete fusion) cross sections for ^{6}Li+^{209}Bi system at energies around the Coulomb barrier, $V_B \simeq 30$ MeV (in c.m.), are available in the literature [24], we chose this reaction for the present study. To have a complete set of data, we decided to measure the elastic, inelastic, transfer and breakup cross sections for the same system. It would be interesting to see whether a simultaneous description of all the channels as well as the energy dependence of the OM potential is possible for the present system (^{6}Li+^{209}Bi) through the same CC calculations with a lot of experimental data for inelastic, transfer, breakup and fusion channels as constraints.

In this article, we present the results of the measurements and analysis of elastic, inelastic, transfer and breakup cross sections for ^{6}Li+^{209}Bi system. Details of the measurements are given in section 2. The analysis and results of exclusive breakup data are given in section 3. Coupled-channels calculations are described in section 4. The optical model data analysis of elastic scattering, discussion on inelastic, transfer, inclusive alpha, fusion and reaction are provided under section 5. Disentangling of various reaction mechanisms to produce alpha particles is made in section 6. Finally, the results are summarized in section 7.

2. Experiment and data analysis

Several experiments were performed using the ^{6}Li beam from the 14-UD Pelletron in Mumbai at near barrier energies, $E_{lab} = 24 - 50$ MeV. Though the experimental setups are almost similar for the above measurements, the details of only the exclusive measurements is described as follows. Exclusive measurements were made only at 40 and 36 MeV. A self-supporting natural Bi target of thickness ≈ 1 mg/cm^2 was employed in the measurement. When the excited ^{6}Li dissociates in-flight into an alpha and deuteron, the fragments are emitted within a cone. The maximum angle [17] between the breakup fragments (α and d) from the decay of ^{6}Li* (3^+, 2.18 MeV) is in the range of θ_{lab}=16°-19° for the ^{6}Li* angular range of 0°-150°. If the two fragment detectors are kept within this cone, there are two possible directions of the alpha (or deuteron) in the rest frame of ^{6}Li that can reach a specified laboratory angle [22, 25] resulting in two peaks in the spectra of alpha (or deuteron). The α and d detectors were kept 10° apart in order to detect each of the breakup fragments with both the peaks arising from sequential breakup corresponding to the above resonant state.

Four telescopes (T_1 to T_4) of Si surface barrier detectors were placed inside a 1-m diameter scattering chamber. Each telescope was provided with a 10 mm diameter collimator to restrict the angular spread to ±1.4°. The "α-telescopes", T_1 and T_3 were optimized for the detection of particles around Z=2-3 by selecting ΔE detectors of 33 μm thickness and E of 500 μm while the "deuteron-telescopes", T_2 and T_4 with thicknesses ΔE=150 μm and E=1000 μm were suitable for the detection of particles around Z=1-3. Coincidences between each α- and deuteron-telescope pair (T_1-T_2, T_2-T_3 and T_3-T_4) were ensured by using individual Time to Amplitude Converters (TACs). Two surface barrier detectors (M_1 and M_2) of thickness 2 mm were placed at ±25° of the beam for normalization and beam monitoring. The inclusive two dimensional spectra of ΔE vs. E (Fig. 1[a,d]) showed good separation of particles with different masses.

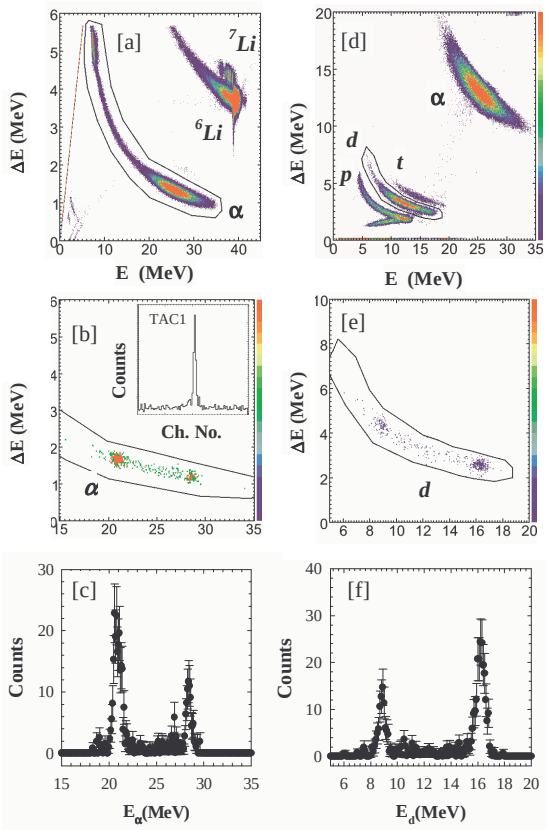

FIG. 1: (Colour online) Typical two dimensional (ΔE vs E) spectra acquired in [a] T_1 (at 55°) and [d] T_2 (at 65°) at 40 MeV beam energy. The resulting spectra after applying coincidence conditions are shown in [b], [c] and [e], [f] respectively. One of the TAC spectra used in gating is shown as an inset in [b].

3. Exclusive breakup data analysis

In the offline analysis, coincidence conditions consisting of two-dimensional gates to select α-particles and deuterons in the corresponding telescopes and a gate around the TAC peak were applied to project inclusive α and d spectra. Fig. 1[a] shows the ungated two-dimensional spectrum in T_1 at θ_α=55°. After applying the coincidence conditions corresponding to the deuteron tele-

scope at θ_d=65° we obtain the projections shown in Figs. 1[b] and [c]. Similarly the two-dimensional spectrum in T_2 at θ_d=65° is shown in Fig. 1[d] and gated projections in Figs. 1[e] and [f]. The α and d spectra show two peaks corresponding to sequential breakup. A small contribution from direct breakup can also be seen in the region between the two peaks of the spectra.

The experimental data for E_α versus E_d and $E_{\alpha d}$ corresponding to the α-d coincidence events when compared to the three-body kinematics[26] show that the two localized peaks in the coincident yields correspond to the projectile breakup through its first resonant state (2.18 MeV, J^π=3$^+$). The α-d coincidence yields corresponding to the two peaks were used to calculate the differential breakup cross sections in the centre-of-mass system at various angles, assuming isotropic emission of the breakup fragments in the rest frame of ^{6}Li and using the formulation of Ref. [27]. The experimental α+d breakup cross section thus obtained are shown as solid circles in Fig. 2 and published in Ref. [28].

In addition to sequential breakup, the differential cross sections for direct breakup were extracted considering relative energies, $E_{\alpha d}$ from the minimum ($\sim$ 0.25 MeV) upto 0.71 MeV excluding the contributions from the peaks attributed to sequential breakup. The average direct breakup cross sections obtained for each angle set are shown as filled diamonds in Fig. 2. The data reveals that direct breakup for the present beam energies is smaller by about one order of magnitude compared to the sequential breakup. The inclusive α cross sections were also extracted and shown as open squares in Fig. 2. It can be seen that the sequential α+d breakup cross sections (filled circles) are about one order of magnitude less than the inclusive α breakup production. A large fraction of α counts in the spectra of T_1 (T_3) were found to be produced in coincidence with protons detected in T_2 (T_4). As observed in Ref. [22], this is mostly due to 1n transfer (^{6}Li+^{209}Bi$\rightarrow^5$Li+^{210}Bi+Q_{opt}) followed by breakup of ^{5}Li ($\rightarrow \alpha$+p +1.97 MeV). Breakup cross sections for α+p channel were

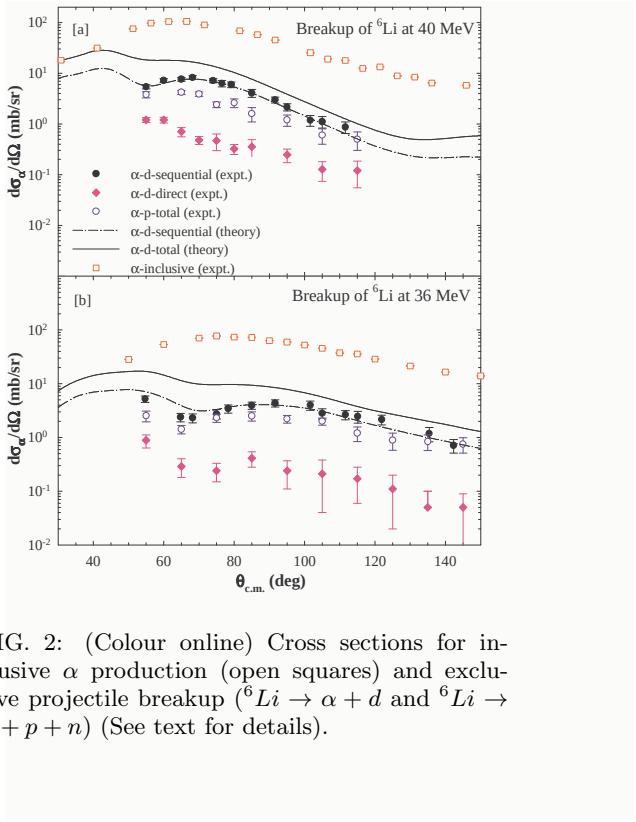

FIG. 2: (Colour online) Cross sections for inclusive α production (open squares) and exclusive projectile breakup ($^6Li \rightarrow \alpha + d$ and $^6Li \rightarrow \alpha + p + n$) (See text for details).

deduced from the data (open circles in Fig. 2) which were found to be much higher than the direct and comparable to the sequential $\alpha + d$ breakup.

4. Coupled-channels calculations

Continuum discretized coupled-channels (CDCC) method was used to calculate the cross sections for elastic and breakup channels with the code FRESCO [29]. For ^{6}Li, couplings to the 3$^+$ (E_x=2.18 MeV), 2$^+$ (E_x=4.31 MeV), and 1$^+$ (E_x=5.65 MeV) resonant states as well as couplings to the non-resonant continuum were included. The continuum up to an excitation energy of 8 MeV with α-d relative momentum L=0, 1 and 2 was included in the coupling. For s and p waves, the continuum was discretized into 16 bins of equal width in the momentum of αd relative motion. In the presence of resonances for d-waves, the discretization of the continuum was slightly modified in order to avoid double counting. The couplings of the ground state to the con-

tinuum as well as continuum to continuum have been included.

CDCC calculations were performed using cluster-folded (CF) interaction [30], where α-target ($V_{\alpha+Bi}$) and deuteron-target (V_{d+Bi}) optical potentials were evaluated at $E_\alpha \approx \frac{2}{3}E_{6Li}$ and $E_d \approx \frac{1}{3}E_{6Li}$, respectively. The $V_{\alpha+Bi}$ potential used in our calculations was taken from Ref. [32] for E_{lab}=24.8 MeV. Similarly, the V_{d+Bi} potential was taken to be same as that of d+^{208}Pb at 12 MeV [33]. Imaginary parts of $V_{\alpha+Bi}$ and V_{d+Bi} describe the removal of flux whenever the individual fragments themselves breakup, excite, or fuse with the target. The strength of the real part of $V_{\alpha+Bi}$ as well as V_{d+Bi} was scaled by a factor of 0.8, compared to the values in Refs. [32, 33], in order to explain the elastic data for both 40 and 36 MeV. The $\alpha + d$ binding potential in ^{6}Li was obtained from Ref. [34].

The results of the CDCC calculations are shown in Figs. 2 and 3 which reproduce the experimental data very well. It can be seen from Fig. 3(a) that the coupling of the breakup channels has a very large effect on elastic scattering. In Fig. 3(b), the calculations with Coulomb coupling, nuclear coupling and Coulomb+nuclear coupling are shown as dashed, dashed-dot-dot and solid lines respectively. It was found that the breakup cross sections calculated with Coulomb+nuclear couplings reproduces the experimental data very well. One can see that nuclear coupling is necessary in order to explain the data particularly at the backward angles, making its effect very prominent. The total α-d breakup (solid lines in Fig. 2) for both the resonant and the non-resonant continuum, calculated up to an excitation energy of 8 MeV (which also includes the undetected α-d breakup contribution), was found to be far less than the inclusive α.

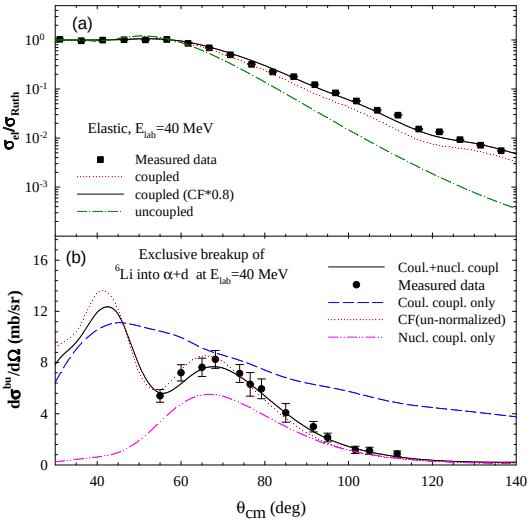

FIG. 3: (Colour online) (a) Exclusive breakup cross section (filled circles) in centre -of-mass frame measured at 40 MeV. Solid, dashed and dashed-dot-dot lines represent the result of CDCC calculations with Coulomb+nuclear, only Coulomb and only nuclear coupling respectively. Dotted line represents the calculation with un-normalized CF potential. (b) Elastic scattering angular distribution at E_{lab}=40 MeV. The results of CDCC calculation with full couplings and normalized (un-normalized) cluster-folded potential is represented by solid line (dotted line). Dashed-dot line was obtained with normalized CF potential but without any breakup coupling.

5. Energy dependence

A. Elastic scattering and OM potential

The measured elastic scattering data were analyzed by the optical model following the formalism described in Refs. [3, 4]. The real and imaginary potentials are calculated at the average strong absorption radius, R_{sa}=12.4 fm. and plotted as a function of bombarding energy in Fig. 4. The consistency between the real and the imaginary potentials (solid lines) was tested by a dispersion relation [35]. From this it can be concluded that there is no pronounced energy dependence or so called "threshold anomaly" of the real potential at energies around the Coulomb barrier, similar to the observations made earlier[5–7, 9, 11] for the reactions involving weakly bound ^{6}Li and ^{9}Be projectiles. As we go down in energy below the Coulomb barrier, the imaginary potential starts increasing (typical of "Breakup threshold anomaly") and it does not reduce to zero even at $E_{lab} \simeq 0.8V_B$, indicating the

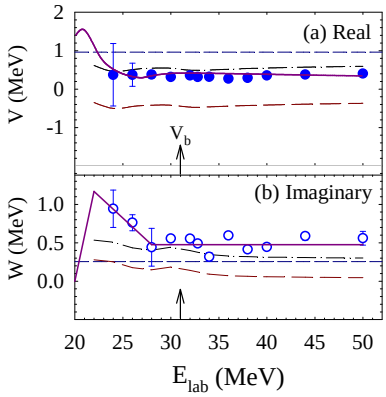

FIG. 4: (Color online) (a) The real and (b) the imaginary potentials (filled and hollow circles respectively) obtained from OM analysis at strong absorption radius, R_{sa} = 12.4 fm. The solid lines are obtained from the dispersion relation. Results from the CC calculations for real (imaginary) part of the bare potential V_{bare} (W_{bare}), dynamic polarization potential ΔV_p (ΔW_p) and effective potential, V_{eff}=ΔV_p+V_{bare} (W_{eff}=ΔW_p+W_{bare}) are represented by short-dashed, medium-dashed and dash-dotted lines respectively.

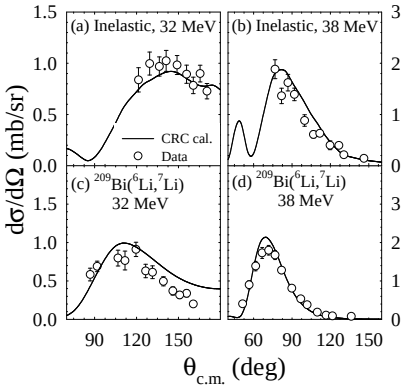

FIG. 5: Measured cross sections along with the CRC calculations for target inelastic state (2.6 MeV) at E_{beam}= (a) 32 and (b) 38 MeV. Cross sections for transfer reaction (^{6}Li,^{7}Li) at above energies are shown in (c) and (d) respectively (see text for details).

presence of some open reaction channel.

The mean component of the dynamic polarization potential (DPP) generated due to breakup couplings was calculated using FRESCO as described in Ref. [36]. In Fig. 4, the average polarization potential (medium dashed line) along with the bare potential (short dashed line) is compared with the OM potential obtained from fit. The real part of the polarization potential ΔV_p calculated at r=12.4 fm was found to be positive at all the energies. It can be observed that the sum of the bare potential and DPP, represented by the dash-dotted lines, reproduces the trend of experimental values of both real and imaginary potentials. One can observe the trend of the imaginary part of the polarization potential particularly at energies below the barrier, where it becomes more and more attractive as we go down in energy and explains the energy dependence of the OM potential at this region.

B. Target inelastic and transfer channels

To see the effect of target inelastic states and transfer channels, coupled reaction channels (CRC) calculations are performed using the CDCC derived effective potentials ($\Delta V_p + V_{bare}$ and $\Delta W_p + W_{bare}$ that includes the effect of projectile breakup) for the entrance channel. Similar to Ref. [4], we have coupled (i) seventeen inelastic states corresponding to the multiplets of ^{208}Pb(3^- and 5^-)$\bigotimes \pi h_{9/2}$, and (ii) transfer couplings that include only low lying excited states of the outgoing transfer partitions with 6 channels for 1-n pickup (^{7}Li+^{208}Bi), 2 channels each for 1-n stripping (^{5}Li+^{210}Bi) and 1-p stripping (^{5}He+^{210}Po) reactions. The β values[37] and the deformation lengths are same as those used in Ref. [4].

Typical results for inelastic states corresponding to ^{208}Pb(3^-)$\bigotimes \pi h_{9/2}$ multiplets are compared with present data at 32 MeV and 38 MeV in Fig. 5(a) and (b) respectively. Results for transfer reaction ^{209}Bi(^{6}Li,^{7}Li) corresponding to g.s. of ^{7}Li and g.s. plus 1st excited state of ^{208}Bi are compared with the present data in Fig. 5(c) and (d). A reasonable description of the above data along with elastic scattering ensures that

the potential parameters used for CDCC calculations are not arbitrary rather highly restricted by the measured elastic, inelastic and transfer angular distributions. The effect of coupling of target inelastic states and transfer reactions on elastic scattering were found to be insignificant. So, the repulsive DPP generated in CDCC calculations due to breakup coupling seems to be the main reason for the absence of normal threshold anomaly in the present system.

C. Inclusive alpha, fusion and reaction

In a typical 1D-projection of α-spectrum measured at any energy, a broad ($\sim$ 8-10 MeV) but distinct alpha peak, with centroid equal to two-third of the projectile energy, was found to be due to the projectile breakup (^{6}Li$\rightarrow \alpha + d$). The yields under these peaks provides the angular distributions of the inclusive breakup alpha, the maximum of which occurs at grazing angles. In Fig. 6, the angle integrated cross sections of inclusive breakup-α (hollow triangles-up) are compared with the cross sections for total reaction σ_R (hollow circles) obtained from OM fit[38], CF (stars)[24] and CF+ICF (hollow triangles-down)[24]. It shows that inclusive breakup is the major reaction channel at energies near and below the Coulomb barrier, and the sum of σ_{CF} and σ_α^{incl} (hollow squares) was found to exhaust all of σ_R predicted by OM.

To calculate the fusion cross sections using FRESCO, two methods were employed. The solid line corresponds to the results by barrier penetration model (BPM) using incoming wave boundary condition as done by Rusek *et al.* [39], and dashed line represents the fusion simulated by cumulative absorption in long ranged imaginary potential. At energies above the Coulomb barrier, it is observed that the BPM fusion matches very well with the total fusion(TF=CF+ICF). But the CF data is found to be smaller by $\sim$30-40% which is in agreement with the conclusions drawn in Ref.[24]. However, at low energies, the CF data compares well with the calculated BPM fusion and shows no suppression. TF cross sections predicted by the cumulative absorption (dashed line) were found to overestimate the experimental data. However, a good reproduction of elastic scattering data by the same CDCC calculations implies that the additional flux absorbed by the imaginary potential ($\sigma_{abs} - \sigma_{TF}$) must be equivalent to the sum of reaction cross sections of target-inelastic and transfer channels that are not included in the CDCC calculations.

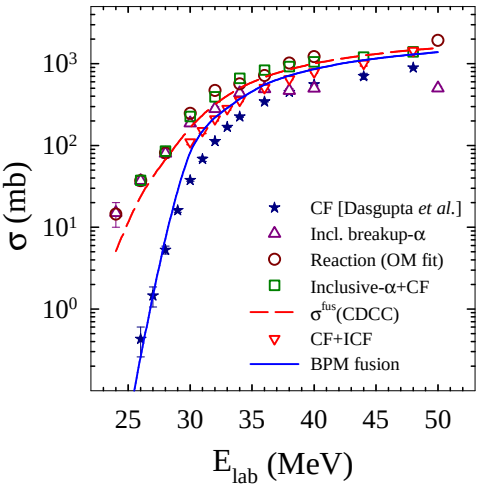

FIG. 6: (Color online) Fusion cross sections obtained from FRESCO by cumulative absorption(dashed line) and by BPM (solid line) are compared with TF, CF, inclusive alpha and σ_R.

D. Energy dependence of reaction channels

To investigate the energy dependence behavior of different reactions, the probabilities of all the significant channels with respect to total reaction cross sections at different energies are compared in Fig. 7. The dominant reaction channels were found to be inclusive breakup-α (hollow diamonds), CF (triangles down) and ICF (stars). At sub-barrier energies, it was interesting to find that while going down in energy, the contributions of σ_α^{incl} and σ_{ICF} to σ_R increase and their trend is just opposite to that of CF, inelastic (dash-dot line) and transfer (dashed line) cross sections. The non-capture breakup cross section (solid line) behavior calculated by the CDCC

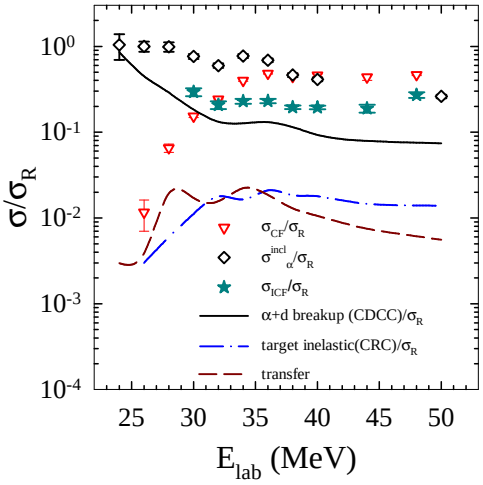

FIG. 7: (Color online) The ratios of cross sections for experimental CF, inclusive alpha and ICF, and calculated exclusive $\alpha + d$ breakup, target inelastic and transfer channels to total reaction cross section (σ_R) showing their relative contributions at different energies.

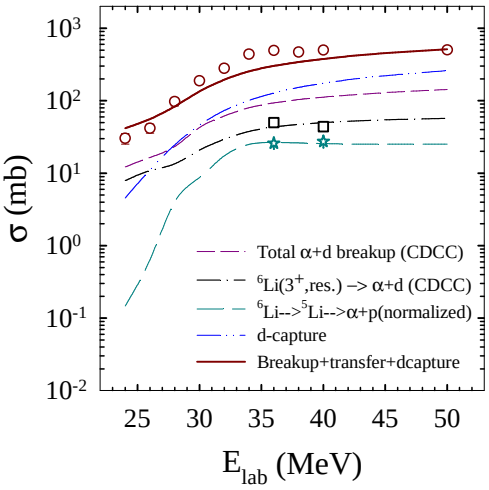

FIG. 8: (Color online) Inclusive breakup alpha (circles, present data) and α contributions from different transfer and breakup channels (see text for details). Squares and stars represent data on exclusive '$d + \alpha$' (sequential) breakup and '$p + \alpha$' breakup[28] respectively.

method is also found to be similar to σ_α^{incl}. This may imply that when all the other channels start closing at sub-barrier energies, the breakup channel does not close possibly due to the small breakup threshold energy of ^{6}Li and the breakup can be caused by even Coulomb excitation. Thus it explains why the imaginary part of the optical potential does not vanish even much below the Coulomb barrier.

6. Disentangling alpha contributions

To unfold the production mechanisms for such a large cross section for σ_α^{incl}, the coupled-channels calculations along with the experimental data were compared as shown in Fig. 8. Following reactions can contribute to the α-production: (i) non-capture breakup of ^{6}Li $\rightarrow$ $\alpha + d$, (ii) $\alpha + d$ breakup followed by d-capture (part of ICF), (iii) neutron stripping followed by breakup (^{6}Li $\rightarrow^5$Li $\rightarrow$ $\alpha + p$), (iv) proton stripping followed by breakup (^{6}Li $\rightarrow^5$He $\rightarrow$ $\alpha + n$), (v) deuteron stripping (^{6}Li,α), and (vi) neutron pickup followed by breakup (^{6}Li $\rightarrow^7$Li $\rightarrow$ $\alpha + t$). However, the major contributions to inclusive α-production were found to be the first three processes. Present calculations and exclusive measurements reported in Ref. [28] show that contributions from last three processes are negligible.

CDCC calculations show that the total (direct + sequential) non-capture '$\alpha + d$' breakup (dashed line) is dominated by the sequential breakup through 3^+ resonance state of ^{6}Li (dot-dashed line). The d-capture (α-emission) cross section, estimated from ICF data by calculating the ratios of Wong model fusion for d+^{209}Bi to α+^{209}Bi at same beam velocity, is also shown in Fig. 8 as a dash-dot-dot line. Maximum contribution from the transfer reactions found to come from the '^{6}Li$\rightarrow^5$Li$\rightarrow$ $\alpha + p$' process (long-dashed line). Combined cross section of total '$\alpha + d$', '$\alpha + p$' (normalized) and d-capture, shown by a solid line, was found to be pretty close to the measured σ_α^{incl}. It is for the first time that the pro-

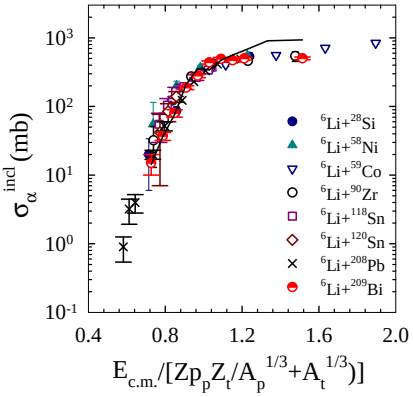

FIG. 9: (Color online) Inclusive breakup alpha cross sections involving ^{6}Li projectile with several different targets including ^{209}Bi (present data) as a function of $E_{c.m.}/[Z_pZ_t/(A_p^{1/3}+A_t^{1/3})]$. The solid line represents the values of '$\sigma_R - \sigma_{CF}$' for ^{6}Li+^{209}Bi.

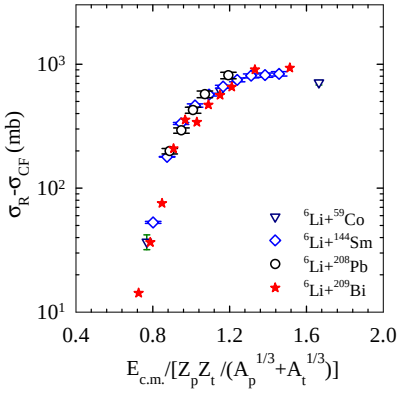

FIG. 10: (Color online) The difference in reaction and CF cross sections ($\sigma_R - \sigma_{CF}$) for several systems involving ^{6}Li as a projectile as a function of $E_{c.m.}/[Z_pZ_t/(A_p^{1/3}+A_t^{1/3})]$.

duction mechanisms of most of the inclusive α particles over a range of beam energies are understood and their contributions are disentangled.

A comparison of the σ_α^{incl} versus reduced energies for several targets involving ^{6}Li as a projectile shows that the cross sections are independent of the target as shown in Fig. 9. Assuming the alpha production to be the dominant direct reaction mechanism, the difference in the reaction and the CF cross sections "$\sigma_R - \sigma_{CF}$" for several reactions was plotted in Fig. 10. Interestingly they also shows exactly the same behavior as in Fig. 9. Although σ_{CF} and σ_R did not show a similar behavior.

7. Summary

Systematic cross sections for elastic, inelastic, transfer and inclusive breakup channels have been measured for ^{6}Li+^{209}Bi reaction at energies $E_{lab} = 24 - 50$ MeV. Exclusive breakup cross sections were also measured at two energies: 36 and 40 MeV to estimate the non-capture breakup contributions towards inclusive data. OM potentials obtained from the elastic scattering angular distribution data shows breakup threshold anomaly in its energy dependence behavior. Imaginary potential was found to remain non-zero at deep sub-barrier energies due to the presence of breakup channels. From CDCC calculations, the dynamic polarization potential generated due to breakup coupling was found to explain the observed energy dependence.

Inclusive alpha cross section was found to be the major reaction channel particularly at sub-barrier energies where it exhausts almost all of the reaction cross section. Comparison of the relative contribution of the different reaction channels (i.e., CF, ICF, inclusive alpha, breakup, inelastic and transfer) towards the total reaction cross section reveals that while going down in energy the contribution of the channels due to projectile breakup (i.e., non-capture breakup and ICF) increases in contradiction to the other channels like CF, inelastic and transfer that get closed at sub-barrier energies. This may imply that the existence of the non-zero reaction cross section or imaginary potential at these energies is due to projectile breakup channels.

A search for the origin of a large inclusive alpha production cross section shows that most of the alpha particles are due to breakup, where either the complementary breakup fragment i.e. d is captured and α is emitted or

both of the fragments are emitted. A comparison of the σ_{α}^{incl} versus reduced energies for several targets involving ^{6}Li as a projectile shows that the cross sections are independent of the target. Interestingly, the difference between reaction and complete fusion cross sections "$\sigma_R - \sigma_{CF}$" also shows exactly the same behavior.

References

[1] G. Baur *et al.*, Nucl. Phys. A **458**, 188 (1986).
[2] C. Mahaux *et al.*, Nucl. Phys. A **449**, 354 (1986).
[3] S. Santra *et al.*, Phys. Rev. C **64**, 024602 (2001).
[4] S. Santra *et al.*, Phys. Rev. C **60**, 034611 (1999).
[5] N. Keeley *et al.*, Nucl. Phys. **A571**, 326 (1994).
[6] A. M. M. Maciel *et al.*, et al., Phys. Rev. C **59**, 2103 (1999).
[7] F. A. Souza *et al.*, Phys. Rev. C **75**, 044601 (2007).
[8] A. Pakou *et al.*, et al., Phys. Rev. C **69**, 054602 (2004).
[9] C. Signorini *et al.*, et al., Phys. Rev. C **61**, 061603(R) (2000).
[10] S. B. Moraes *et al.*, Phys. Rev. C **61**, 064608 (2000).
[11] P. R. S. Gomes *et al.*, et al., Phys. Rev. C **71**, 034608 (2005).
[12] M. S. Hussein *et al.*, Phys. Rev. C **73**, 044610 (2006).
[13] R. J. Woolliscroft *et al.*, Phys. Rev. C **69**, 044612 (2004).
[14] G. R. Kelly *et al.*, Phys. Rev. C **63**, 024601 (2000).
[15] C. Signorini *et al.*, Eur. Phys. J. A **10**, 249 (2001).
[16] R. J. Woolliscroft *et al.*, Phys. Rev. C **68**, 014611 (2003).
[17] C. Signorini *et al.*, Phys. Rev. C **67**, 044607 (2003).
[18] K. O. Pfeiffer *et al.*, Nucl. Phys. **A206**, 545 (1973).
[19] A. Pakou *et al.*, Phys. Rev. Lett. **90**, 202701 (2003).
[20] H. Kumawat *et al.*, Phys. Rev. C **81**, 054601 (2010).
[21] F. Souza *et al.*, Nucl. Phys. **A821**, 36 (2009).
[22] C. M. Castaneda *et al.*, Phys. Rev. C **21**, 179 (1980).
[23] L. F. Canto *et al.*, Phys. Rep. **424**, 1 (2006).
[24] M. Dasgupta *et al.*, Phys. Rev. C **70**, 024606 (2004).
[25] D. Scholz *et al.*, Nucl. Phys. A **288**, 351 (1977).
[26] H. Fuchs, Nucl. Instrum. Methods **200**, 361 (1982).
[27] R. J. de Meijer and R. Kamermans, Rev. Mod. Phys **57**, 147 (1985).
[28] S. Santra *et al.*, Phys. Lett. B **677**, 139 (2009).
[29] I. J. Thompson, Comp. Phys. Rep. **7**, 167 (1988).
[30] F. G. Perey and G. R. Satchler, Nucl. Phys. A **97**, 515 (1967).
[31] Y. Hirabayashi and Y. Sakuragi, Phys. Lett. B **258**, 11 (1991).
[32] P. Singh *et al.*, Phys. Rev. C **43**, 1867 (1991).
[33] P. R. Christensen *et al.*, Nucl. Phys. A **129**, 337 (1969).
[34] H. Nishioka *et al.*, Nucl. Phys. A **415**, 230 (1984).
[35] G. R. Satchler, Phys. Rep. **199**, 147 (1991).
[36] I. J. Thompson *et al.*, Nucl. Phys. A **505**, 84 (1989).
[37] T. P. Cleary *et al.*, Nucl. Phys. A **232**, 287 (1974).
[38] S. Santra *et al.*, Phys. Rev. C **83**, 034616 (2011).
[39] K. Rusek *et al.*, Phys. Rev. C **70**, 014603 (2004).